

Supplementary Information

Insights into Host-Guest Interactions and Enhanced MRI Contrast Applications of Water-Soluble Tetrahedral Metal- Organic Cages

Yu-Xiao Chen,^{1†} Mao-Song Qiu,^{23†} Jie-Sheng Hu,¹ Hua-Liang Yue,¹ Meng Yu,^{1*} Shi-Zhen Chen,^{234*} Xin Zhou²³⁴ and Jun Tao^{1*}

¹*Key Laboratory of Cluster Science of Ministry of Education, School of Chemistry and Chemical Engineering, Liangxiang Campus, Beijing Institute of Technology, Beijing 102488 China*

²*State Key Laboratory of Magnetic Resonance Spectroscopy and Imaging, National Center for Magnetic Resonance in Wuhan, Wuhan Institute of Physics and Mathematics, Innovation Academy for Precision Measurement Science and Technology, Chinese Academy of Sciences, Wuhan 430071 China.*

³*University of Chinese Academy of Sciences, Beijing 100049 China*

⁴*School of Biomedical Engineering, Hainan University, Haikou 570228 China*

†Equally contributed to this work.

*Corresponding authors: mengyu@bit.edu.cn; chenshizhen@wipm.ac.cn;
taojun@bit.edu.cn

1. Materials and Methods

All reagents and solvents were purchased from commercial sources and used as received without any further purification. NMR spectra were measured on a Bruker Ascend 400M (400 MHz) Fourier transform NMR spectrometer (^1H) and Bruker Ascend 700M (700 MHz) Fourier transform NMR spectrometer (^1H DOSY and 2D NMR) with chemical shifts (δ , ppm) relative to deuterated reagents. High resolution ESI-TOF mass spectra were recorded on AB Sciex Triple ToF 6600 plus mass spectrometers in negative reflection mode. UV-vis absorption spectra were taken on a Shimadzu UV-1900 spectrometer. Cyclic voltammetry was carried out in a standard one compartment cell, equipped with a Glassy Carbon working electrode, a platinum wire as counter electrode and a silver chloride (1M KCl) reference electrode using a CHI 660e potentiostat. ICP-OES was measured on a Agilent ICP-OES 5800. The electron paramagnetic resonance (EPR) spectrum was acquired on a Bruker EMXplus spectrometer. Hydrodynamic diameter and electrokinetic (zeta) potential were carried out in a Malvern Zazo ZS.

Animals

All procedures involving animals were approved by the Animal Welfare and Research Ethics Committee at the Innovation Academy for Precision Measurement Science and Technology, Chinese Academy of Sciences (APM23024T). For the *in vivo* MRI experiments, 8-9-week-old female Balb/c mice (Wuhan Bainte Biotechnology Co., Ltd.) were used. Mice were kept in standard housing conditions with free access to food and water, and a 12-h light/dark cycle.

Magnetic Susceptibility Measurements

Magnetic susceptibility measurement was measured on a Quantum Design MPMS XL7 magnetometer. Powdered sample was loaded into gelatin capsules and inserted into straws for SQUID analysis. Variable-temperature magnetic susceptibilities were measured from 2 to 300 K and 300 to 2 K at 5000 Oe.

EPR Spectroscopy

The EPR spectrum of $\text{K}_{12}[\text{Fe}_4\text{L}_4]$ was acquired in a frozen glass of 10/1 mixture of water and glycerol at 100 K. Data was acquired on a Bruker EMXplus spectrometer operating at 9.419 GHz with a microwave power of 2.000 mW and a modulation amplitude of 1 Gauss. The experimental spectrum was fitted using the EasySpin software package.¹

X-ray Crystallographic Analyses

Single-crystal X-ray diffraction data were recorded with a Bruker ARINAX MD2 diffractometer equipped with a MarCCD-300 detector ($\lambda = 0.71073 \text{ \AA}$) at the BL17B beam line station of the Shanghai Synchrotron Radiation Facility (SSRF). The crystal's temperature

was controlled by an Oxford Cryosystem 800 equipment. Unit cell refinement and data reduction were performed using the HKL3000 software. The structures were solved by direct methods and further refined by full-matrix least-squares techniques on F^2 with SHELX program.²

The crystals of the cage exhibited significant instability under atmospheric conditions. Upon removal from the mother liquor, the crystals rapidly lost the solvent, resulting in chalking or cleavage. To address this issue and select samples suitable for single-crystal analysis, all crystals were picked in fresh solvent and immediately subjected to rapid cooling under cryostream, thereby enhancing the quality of the crystallographic data obtained. Typically, non-hydrogen atoms with occupancies greater than 0.5 were refined anisotropically. Carbon-bound hydrogen atoms were positioned ideally and refined using a riding model. Disorder was addressed using standard crystallographic methods, including constraints, restraints, and rigid bodies, as necessary (e.g., SIMU, DFIX, AFIX).

Specific refinement details:

Pale yellow block crystals, suitable for single crystal diffraction analysis, were obtained by the slow evaporation of a methanol solution of $(\text{NEt})_{12}[\text{Ga}_4\text{L}_4]$. These crystals rapidly lost solvent upon removal from the mother liquor, necessitating careful extraction and immediate immersion in oil to select high-quality specimens. The selected crystals were then wrapped in oil and promptly placed in a cryostream at 100 K to collect low-temperature data. Despite these precautions, solvent loss from the crystal structure compromised their quality, resulting in some ambiguity in electron density and preventing clear resolution of solvent molecules and cations. To obtain reasonable models, AFIX restraints were applied to all benzene rings and triazine rings. The tetraethylammonium cation outside the cage cavity exhibited a high degree of disorder and mutual interference, complicating modeling efforts. Consequently, no NEt_4^+ cation was successfully resolved outside the cage cavity, further indicating solvent loss and poor diffraction properties. Nonetheless, the data quality was sufficient to establish the structural connectivity. The asymmetric unit comprised a tetrahedral cage, a tetraethylammonium counter ion inside the cage, and eleven tetraethylammonium counter ions outside the cage. Therefore, the SQUEEZE function of PLATON was employed to address the electron density contributions of highly disordered solvent molecules and cations that could not be modeled with discrete atomic positions.³ The hydrogen atom positions were fixed geometrically at calculated distances and allowed to ride on the parent atoms. Crystallographic data have been deposited with the CCDC no. 2382639.

Stokes-Einstein Determination of Solute Radius

The cage dimensions can be estimated using the Einstein-Stokes equations as follows,

$$D = \frac{k_B T}{6\pi\mu_m R_0}$$

Where D is the self-diffusion constant ($\text{m}^2\cdot\text{s}^{-1}$) determined by ^1H DOSY, k_B is the Boltzmann constant ($1.38 \times 10^{-23} \text{ J}\cdot\text{K}^{-1}$), R_0 is the van der Waals radius of the molecule (m), μ_m is the viscosity of the mixture calculated as follows,

$$\mu_m = \left(\sum_{i=1}^n x_i \mu_i^{1/3} \right)^3$$

Where x is the ratio of solvent, μ is the viscosity of the solution ($8.9 \times 10^{-4} \text{ Pa}\cdot\text{s}$ for water and $2.0 \times 10^{-3} \text{ Pa}\cdot\text{s}$ for DMSO at 298 K).

VOIDOO calculations

To determine the available void space within $[\text{Ga}_4\text{L}_4]^{12-}$, VOIDOO calculations⁴ were calculated based on the crystal structures, with anions and solvent molecules removed. A virtual probe with a radius of 1.4 Å (default, water size) was used for all MOCs, as were standard parameters taken from published procedures, as follows.⁵

Maximum number of volume-refinement cycles: 30

Minimum size of secondary grid: 3

Grid for plot files: 0.1

Primary grid spacing: 0.1

Plot grid spacing: 0.1

Aqueous Stability

UV-Vis spectra were collected using a Shimadzu UV-1900 spectrometer. To monitor the stability of $\text{K}_{12}[\text{Fe}_4\text{L}_4]$ in solution, we focused on the ligand-to-metal charge transfer (LMCT) from the metal center to the catechol ligand. Spectra were recorded from 350 nm to 750 nm in 1 nm wavelength increments to identify the peak of the LMCT band. The peak absorbance was used as an indicator of solution stability. Spectra were scanned at 30-minute intervals over a period of at least 720 minutes.

PBS Buffer

A 100 μM solution of $\text{K}_{12}[\text{Fe}_4\text{L}_4]$ was prepared in PBS buffer at 37 °C and pH 7.4. The LMCT absorbance peaks were monitored continuously between 350 and 750 nm for 12 hours.

Cations

A 100 μM solution of $\text{K}_{12}[\text{Fe}_4\text{L}_4]$ was prepared in HEPES buffer with 100 mmol NaCl and 40 equivalents of $\text{Zn}(\text{NO}_3)_2$ at 37 °C and pH 7.4. The LMCT absorbance peaks were monitored continuously between 350 and 750 nm for 24 hours.

Anions

A 100 μM solution of $\text{K}_{12}[\text{Fe}_4\text{L}_4]$ was prepared in HEPES buffer with 100 mM NaCl and 400 μM of disodium ethylenediaminetetraacetic acid (EDTA) at 37 $^\circ\text{C}$ and pH 7.4. The LMCT absorbance peaks were monitored continuously between 350 and 750 nm for 24 hours.

HSA

A 100 μM solution of $\text{K}_{12}[\text{Fe}_4\text{L}_4]$ was prepared in PBS buffer with 35 mg/ mL HSA at 37 $^\circ\text{C}$ and pH 7.4. The LMCT absorbance peaks were monitored continuously between 350 and 750 nm for 12 hours.

Ascorbic Acid

A 100 μM solution of $\text{K}_{12}[\text{Fe}_4\text{L}_4]$ was prepared in PBS buffer with 1 mM ascorbic acid at 37 $^\circ\text{C}$ and pH 7.4. The LMCT absorbance peaks were monitored continuously between 350 and 750 nm for 24 hours.

Isothermal Titration Calorimetry (ITC)

The ITC experiment was performed by an isothermal titration microcalorimeter (TA Nano ITC) under atmospheric pressure and at 25.0 $^\circ\text{C}$, giving the association constants (K) and the thermodynamic parameters. A water solution of $\text{K}_{12}[\text{Ga}_4\text{L}_4]$ in a 0.05 mL syringe was sequentially injected with stirring at 250 rpm into a water solution of TEMPO in the sample cell (0.35 mL volume). Raw data for sequential 25 injections (2 μL per injection) of $\text{K}_{12}[\text{Ga}_4\text{L}_4]$ solution (5.0 mM) injecting into TEMPO solution (0.5 mM). The thermodynamic parameters was obtained by using the ‘independent’ model.

Proton Relaxivity Determination

Proton longitudinal relaxation rate constants (R_1) were performed on a 400 MHz NMR spectrometer (Bruker, Germany) at 22 $^\circ\text{C}$ and a 0.5 T Low-field nuclear magnetic resonance spectrometer (LF-NMR) (0.5 T, Niumag, Suzhou) at 32 $^\circ\text{C}$. We used the T1map_RARE sequence for T_1 measurements with the following parameters: Echo Spacing: 8 ms; Rare factor: 2; Repetition Time: 1500 ms; Scan time: 25 min 30 s; T_1 experiments: 6; Repetition Time: 253 400 800 1500 3000 5500 on the 400 MHz NMR spectrometer. And used an inversion-recovery sequence for T_1 measurements with the following parameters: Tw: 3000 ms; NS: 4; NTI: 24 on a 0.5 T LF-NMR.

Protein binding

The interaction between $\text{K}_{12}[\text{Fe}_4\text{L}_4]$ and HSA was assessed by measuring the observed longitudinal relaxation rate (R_{1obs}) at 298 K in a 0.12 mM $\text{K}_{12}[\text{Fe}_4\text{L}_4]$ solution prepared in PBS at pH 7.4. The binding constants of $\text{K}_{12}[\text{Fe}_4\text{L}_4]$ with HSA were determined using the proton relaxation enhancement method. This method considers the relaxation enhancement resulting

from the formation of slowly rotating macromolecular adducts. Consequently, the following equilibria were considered, and the association constants were defined as follows:



where n is the number of independent binding sites and K_a the apparent binding constant.

$$[Fe_4L_4]_{total} = [Fe_4L_4] + [Fe_4L_4HSA]$$

$$R_{1obs} = R_{1p} + R_{1d} = r_1[Fe_4L_4] + r_1^b[Fe_4L_4HSA] + R_{1d}$$

where R_{1obs} is influenced by both diamagnetic (R_{1d}) and paramagnetic (R_{1p}) relaxation.

Additionally, r_1 and r_1^b represent the millimolar relaxivities of Fe_4L_4 in its free form and when bound to HSA, respectively.

$$R_{1obs} = \frac{(K_a[Fe_4L_4]_{total} + nK_a[HSA]_{total} + 1) - \sqrt{(K_a[Fe_4L_4]_{total} + nK_a[HSA]_{total} + 1)^2 - 4K_a^2[Fe_4L_4]_{total}n[HSA]_{total}}}{2K_a} \times (r_1^b - r_1 + r_1[Fe_4L_4]_{total}) \times 1000 + (0.33 \times [HSA]_{total} \times 1000) + 1.0$$

By combining the equations above, we can obtain K_a .

***In Vivo* Safety Analysis**

Healthy Balb/c mice were allocated into two groups: a control group receiving saline and a test group receiving $K_{12}[Fe_4L_4]$ ($n = 3$ per group). The $K_{12}[Fe_4L_4]$ group was administered an intravenous dose of 0.01 mM/kg, while the control group received an equivalent volume of saline (100 μ L) intravenously. After 24 hours, blood samples were collected from the mice by enucleation to obtain serum for subsequent liver and kidney function analyses. Additionally, the mice were dissected to retrieve major organs, including the heart, liver, spleen, lungs, and kidneys, which were then subjected to histological examination using H&E staining.

***In Vivo* MRI Acquisition and Data Analysis**

In vivo MRI experiments were performed on a 9.4 T MR scanner (Bruker, Germany). For the *in vivo* 1H T_1 -weighed MRI, mice were *i.v.* injected with $K_{12}[Fe_4L_4]$ or Prohance (0.01 mM/kg) in the physiological saline. The MRI of mice was acquired pre-injection and 5 min, 40 min, 2 h, 4 h, and 8 h post-injection in the $K_{12}[Fe_4L_4]$ group, while the acquired time point of mice in the Prohance group was set as pre-injection and 5 min, 40 min, and 2 h post-injection. A glass tube containing water was used as an internal reference. After anesthesia with isoflurane, the 1H T_1 -weighed MRI of mice was acquired using a T_1 -RARE imaging sequence (TR = 500 ms, TE = 6 ms, FOV = 3.5 cm \times 3.5 cm, 1 mm slice thickness, RARE factor = 2, matrix size = 256 \times 256, number of averages = 8, resolution = 0.137 \times 0.137 mm/pixel, acquisition time = 8 min 32 s). Subsequently, the acquired MRI data was transferred as DICOM images to a Radiant DICOM Viewer for quantitative image analysis. This contained manual segmentation of the liver, kidneys, and spleen ROI for each slice, slice-wise normalization of mean ROI

signal intensity (SI) with the water reference standard to account for inter-session variability, followed by combining these normalized, slice-wise values to generate mean volumetric liver, kidneys, and spleen MR SI for each time point.

Percentage signal enhancement was calculated using the following formula:

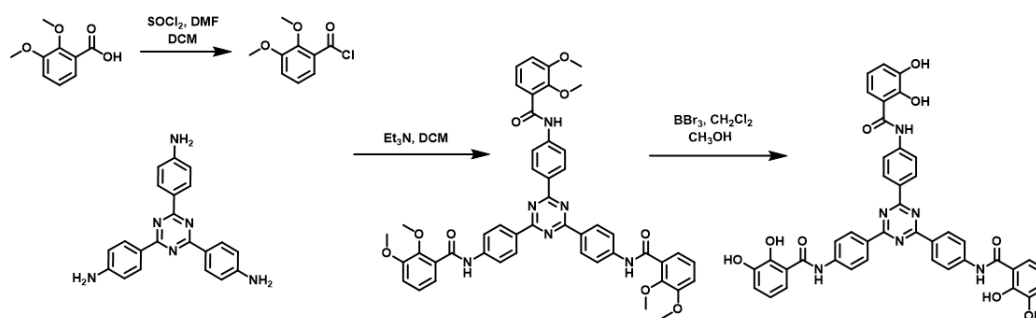
$$\frac{(SI_{\text{post}} - SI_{\text{pre}})}{SI_{\text{pre}}} \times 100$$

where SI_{pre} and SI_{post} represent the signal intensities in T_1 -weighted MR images pre- and post-injected with $K_{12}[Fe_4L_4]$ or Prohance, respectively.

Statistical Analysis

The data are expressed as mean \pm SEM. All statistical calculations were performed using GraphPad Prism 9.0.

2. Synthesis and Characterization



Scheme S1. Synthesis of H_6L .

Synthesis of 2,3-dimethoxy-benzoyl chloride

To a mixture of 2,3-dimethoxy-benzoic acid (3.00 g, 16.5 mmol) and dry dichloromethane (15 mL) was added dropwise thionyl chloride (1.44 mL, 19.8 mmol) under nitrogen and stirring. Then a catalytic amount of *N,N*-dimethylformamide was added. The solution was stirred at 40 °C for 12 hours. The volatiles were removed to afford the pale yellow waxy solid (3.04 g, 15.2 mmol) with 92% yield. The crude product 2,3-dimethoxy-benzoyl chloride was used without further purification.

Synthesis of *N*-{4-[4,6-bis(4-((2,3-dimethoxyphenyl)carbonyl)amino)phenyl]-1,3,5-triazin-2-yl}phenyl}-2,3-dimethoxybenzamide (Me_6L)

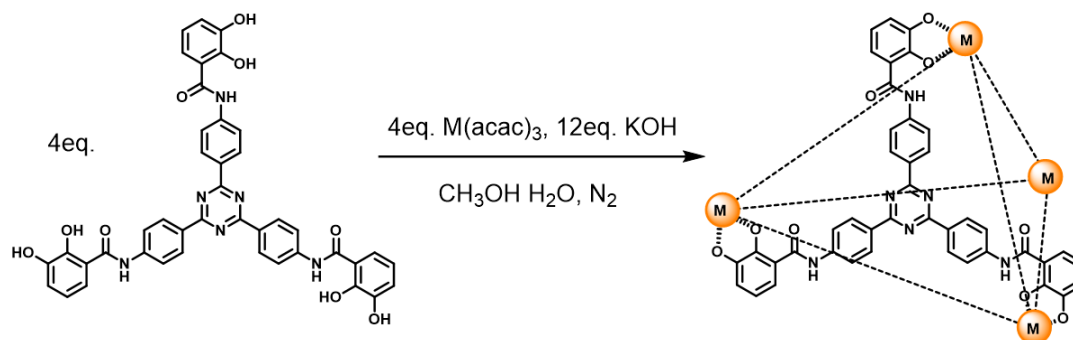
To a mixture of 2,3-dimethoxy-benzoyl chloride (2.4 g, 12 mmol) and 2,4,6-(4-aminophenyl)-1,3,5-triazine (1.2 g, 3.4 mmol) in CH_2Cl_2 under nitrogen and stirring. Then NEt_3 (5 mL, 36 mmol) was added. The suspension was stirred at room temperature for 12 hours. The white precipitate was collected by vacuum filtration and washed with cold water

three times to produce Me₆L (2.31 g, 2.72 mmol) with 80% yield. ¹H NMR (400 MHz, DMSO-*d*₆) δ 10.64 (s, 3H), 8.74 (d, *J* = 8 Hz, 6H), 8.03 (d, *J* = 8 Hz, 2H), 7.25–7.15 (m, 9H), 3.88 (s, 9H), 3.85 (s, 9H). ¹³C NMR (400 MHz, DMSO-*d*₆) δ 170.18, 165.35, 154.01, 145.90, 142.89, 130.84, 130.78, 129.32, 123.84, 120.04, 118.28, 113.71, 61.70, 52.63.

Synthesis of *N*-{4-[4,6-bis(4-[(2,3-dihydroxyphenyl)carbonyl]amino}phenyl)-1,3,5-triazin-2-yl]phenyl}-2,3-dihydroxybenzamide (H₆L)

Me₆L (0.636 g, 0.75 mmol) was added to 30 mL CH₂Cl₂. Nitrogen was bubbled to the mixture for 20 minutes with stirring. The mixture was allowed to stand in -78 °C before adding 1 M BBr₃ (18 mL, 18 mmol) in CH₂Cl₂ dropwise. The suspension was stirred at room temperature for 12 hours. Then the reaction was quenched by the addition of 200 mL methanol. The solvent was removed to afford the crude product. Then the crude product was washed with methanol three times to produce H₆L as pale yellow powder (0.439 g, 0.585 mmol) with 78% yield. ¹H NMR (400 MHz, DMSO-*d*₆) δ 11.31 (s, 3H), 11.68 (s, 3H), 9.56 (s, 3H), 8.77 (d, *J* = 12 Hz, 6H), 8.04 (d, *J* = 8 Hz, 6H), 7.45 (d, *J* = 8 Hz, 3H), 7.01 (d, *J* = 8 Hz, 3H), 6.82 (t, *J* = 20 Hz, 3H). ¹³C NMR (400 MHz, DMSO-*d*₆) δ 170.22, 167.67, 147.81, 146.21, 142.61, 130.86, 129.62, 120.54, 119.10, 118.78, 118.66, 117.85. Maldi-TOF-MS *m/z* = 763.2728 [H₆L+H]⁺.

Synthesis of K₁₂[Fe₄L₄]



Scheme S2. Synthesis of M₄L₄.

H₆L was suspended in a methanol/water (v/v = 1/1) mixture and bubbled under nitrogen atmosphere for 30 minutes to remove dissolved oxygen from the solvent. Subsequently, an aqueous solution of potassium hydroxide (0.25 mL, 0.6 M) was added under magnetic stirring and the insoluble H₆L (0.038 g, 0.05 mmol) gradually dissolved into a pale yellow solution. Then Fe(acac)₃ (0.018 g, 0.05 mmol) was added and the solution immediately turns blackish brown. The mixture was heated at 80 °C overnight, then was returned to room temperature and centrifuged to remove precipitate to obtain a dark red solution. Volatiles were removed under reduced pressure to give black solid as the crude product. The crude product was dissolved in 1 mL of a methanol/water mixture (9/1), and the product was precipitated by adding 30 mL of

diethyl ether as $K_{12}[Fe_4L_4]$ (0.046 g, 0.012 mmol) in 96% yield. ESI(-)-Q-TOF-MS in water $m/z = 660.4367 [Fe_4L_4-K^+-H^{6+}]^{5-}$, $m/z = 825.5464 [Fe_4L_4-K^+-H^{7+}]^{4-}$, $m/z = 1100.3915 [Fe_4L_4-K^+-H^{8+}]^{3-}$, $m/z = 1650.0910 [Fe_4L_4-K^+-H^{9+}]^{2-}$. Purity (96%) was determined by ICP-OES analysis for iron content.

Synthesis of $K_{12}[Ga_4L_4]$

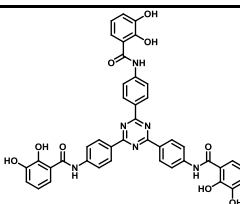
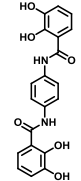
Synthesis of $K_{12}[Ga_4L_4]$ followed the same procedure of $K_{12}[Fe_4L_4]$ by replacing $Fe(acac)_3$ with $Ga(acac)_3$. Upon addition of $Ga(acac)_3$ the mixture rapidly turned yellow. After 8 hours, the mixture was centrifuged to remove precipitate to obtain a pale yellow solution. Volatiles were removed under reduced pressure to yield yellow solids as the crude product. The crude product was dissolved in 1 mL of a methanol/water mixture (9/1), and the product was precipitated by adding 30 mL of diethyl ether as $K_{12}[Ga_4L_4]$. 1H NMR (400 MHz, D_2O) δ 8.20–7.92 (br, 48H), 7.28 (d, $J = 8.00$ Hz, 12H), 6.87 (d, $J = 8.00$ Hz, 12H), 6.65 (t, $J = 8.00$ Hz, 12H).

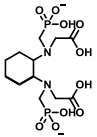
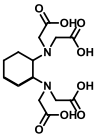
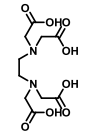
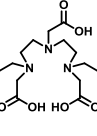
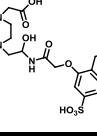
Synthesis of $(NEt_4)_{12}[Ga_4L_4]$

Synthesis of $(NEt_4)_{12}[Ga_4L_4]$ followed the same procedure of $K_{12}[Ga_4L_4]$, except for the additional addition of NEt_4Cl . 1H NMR (700 MHz, $D_2O/DMSO-d_6$) δ 9.05 (d, $J = 12$ Hz, 12H), 8.65 (d, $J = 5.46$ Hz, 12H), 7.88 (d, $J = 6.79$ Hz, 12H), 7.22 (d, $J = 8.12$ Hz, 12H), 6.98 (d, $J = 7.56$ Hz, 12H), 6.82 (d, $J = 7.14$ Hz, 12H), 7.01 (t, $J = 7.00$ Hz, 12H).

3. Additional Table

Table S1. Water proton longitudinal relaxivity r_1 values for Fe(III) and Gd(III) complexes normalized to complex concentration in the absence or presence of HSA.

Ligand structures	Complex	0.5 T		9.4 T		other	
		Water	with albumin	Water	with albumin	Water	with albumin
	$K_{12}[Fe_4L_4]$	6.17	14.17	5.51	7.57		
	FeL_1^a					0.88 (1 T)	
	$Fe_2L_2^b$					1.07 (1 T)	
	$Fe_4L_3^c$					5.72 (1 T)	

				8.3 ± 0.2 (1.4 T)	26 ± 0.1 (1.4 T)
	Fe ₄ L ₆ ^c			8.7 ± 0.2 (4.7 T)	21 ± 0.3 (4.7 T)
	Fe-tBPCDTA	1.17 ± 0.01	1.45 ± 0.06 ^d	1.47 ± 0.12	
	Fe-tCDTA	2.27 ± 0.04	2.46 ± 0.05 ^d	2.62 ± 0.17	
	Fe-EDTA	1.56 ± 0.01	1.60 ± 0.01 ^d	1.82 ± 0.09	
	Gd-DTPA	4.27 ± 0.01		2.72 ± 0.12	
	Gd-L ⁴ ^e	7.1	26.5		

^a L¹ = catecholate. ^b L² = 3-[[4-[[[(2,3-dioxidophenyl)carbonyl]amino} phenyl]amino]carbonyl} benzene-1,2-diolate. ^c L³ = 3-[[5-[[[(2,3-dioxidophenyl) carbonyl]amino]-1-naphthyl]amino]carbonyl} benzene-1,2-diolate. ^d With bovine serum albumin (BSA). ^e L⁴ = HPDO3A-trisulfonated pyrene

Table S2. Crystal data and structural refinements for (NEt₄)₁₂[Ga₄L₄].

	(NEt ₄) ₁₂ [Ga ₄ L ₄]
CCDC	2382639
Formula	C ₁₇₆ H ₁₁₆ Ga ₄ N ₂₅ O ₃₆
Formula weight	3435.81
Temperature / K	100
Crystal system	trigonal
Space group	R $\bar{3}$
<i>a</i> / Å	67.41(3)
<i>b</i> / Å	67.41(3)
<i>c</i> / Å	34.457(7)
<i>α</i> / °	90
<i>β</i> / °	90
<i>γ</i> / °	120
<i>V</i> / Å ³	135599(124)
<i>Z</i>	18
<i>ρ</i> / g cm ³	0.757
<i>μ</i> / mm ⁻¹	0.400
<i>F</i> (000)	31662.0

Crystal size/mm ³	0.15 × 0.05 × 0.03
Radiation	synchrotron (λ = 0.71073)
2θ range for data collection / °	1.372 to 29.4
Index ranges	-46 ≤ h ≤ 45, -48 ≤ k ≤ 26, -23 ≤ l ≤ 24
Reflections collected	32873
Independent reflections	11319 [R _{int} = 0.1454, R _{sigma} = 0.1106]
Data / restraints / parameters	11319 / 1651 / 1849
Goodness-of-fit on F ²	1.790
Final R indexes [I >= 2σ (I)]	R ₁ = 0.1415, wR ₂ = 0.4033
Final R indexes [all data]	R ₁ = 0.1669, wR ₂ = 0.4280
Largest diff. peak/hole / e Å ⁻³	0.63/-0.36

$${}^a R_1 = \frac{\sum ||F_o| - |F_c||}{\sum |F_o|} \quad {}^b wR_2 = \left\{ \frac{\sum [w(F_o^2 - F_c^2)^2]}{\sum [w(F_o^2)^2]} \right\}^{1/2} .$$

Table S3. The bond distance of (NEt₄)₁₂[Ga₄L₄].

Ga1–O1	1.948(19)	Ga3–O13	1.938(16)
Ga1–O2	1.88(2)	Ga3–O14	1.932(15)
Ga1–O3	2.09(3)	Ga3–O15	1.996(14)
Ga1–O4	1.90(2)	Ga3–O16	2.048(15)
Ga1–O5	1.93(2)	Ga3–O17	2.019(15)
Ga1–O6	2.032(19)	Ga3–O18	2.029(14)
Ga2–O7	1.95(2)	Ga4–O19	1.982(19)
Ga2–O8	1.95(2)	Ga4–O20	1.880(18)
Ga2–O9	2.17(2)	Ga4–O21	2.066(19)
Ga2–O10	1.94(2)	Ga4–O22	1.99(2)
Ga2–O11	2.01(2)	Ga4–O23	2.03(2)
Ga2–O12	1.98(2)	Ga4–O24	1.994(18)

3. Additional Figures

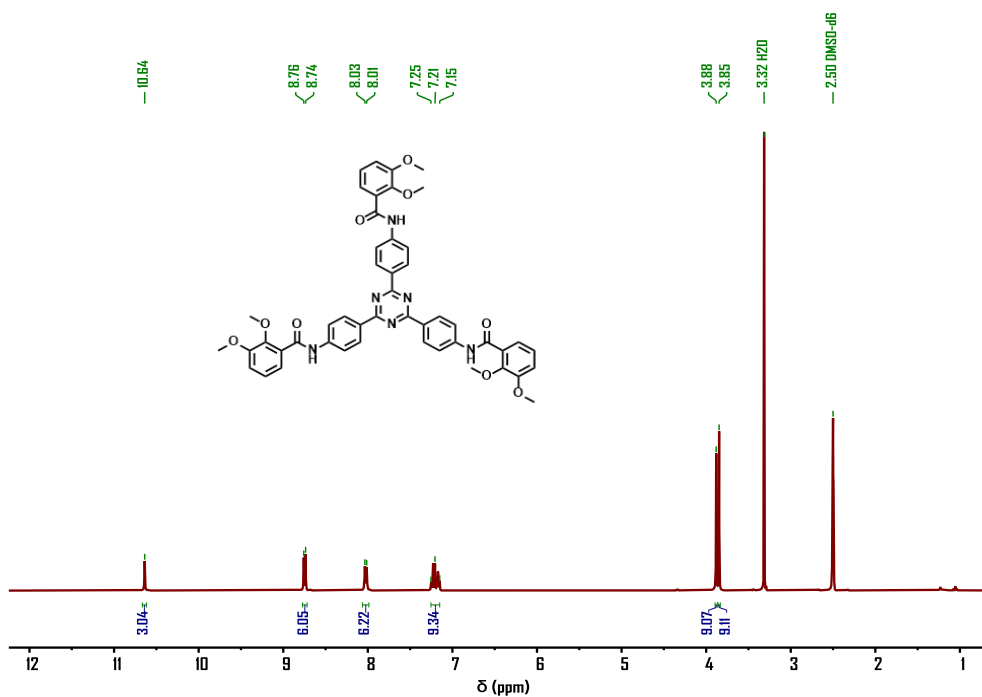


Figure S1. ¹H NMR (400 MHz, DMSO-*d*₆) of Me₆L.

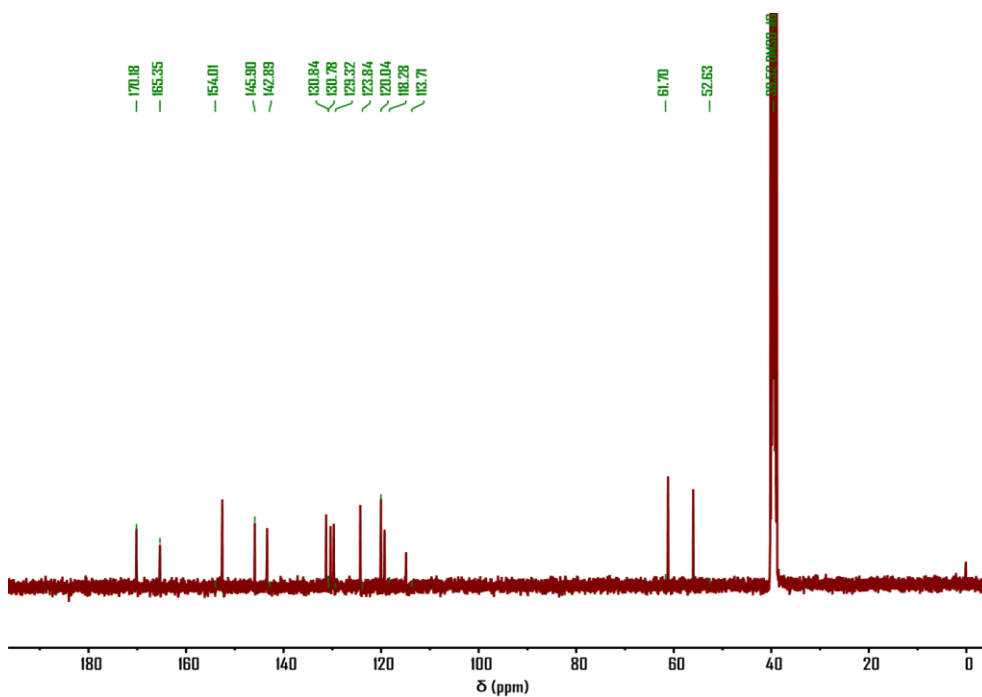


Figure S2. ¹³C NMR (400 MHz, DMSO-*d*₆) of Me₆L.

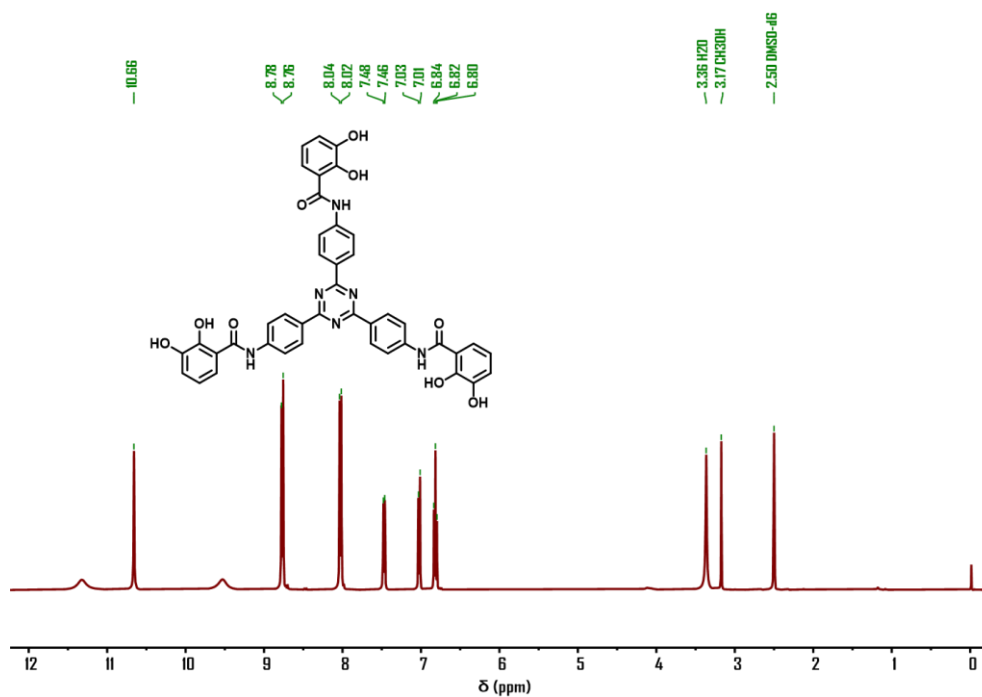


Figure S3. ¹H NMR (400 MHz, DMSO-*d*₆) of H₆L.

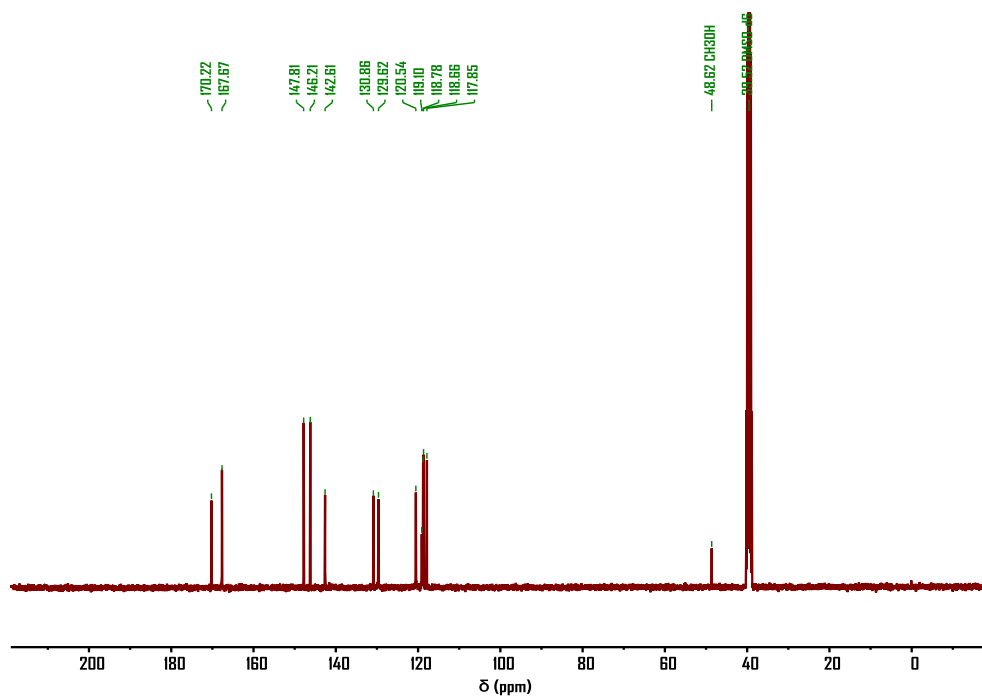


Figure S4. ¹³C NMR (400 MHz, DMSO-*d*₆) of H₆L.

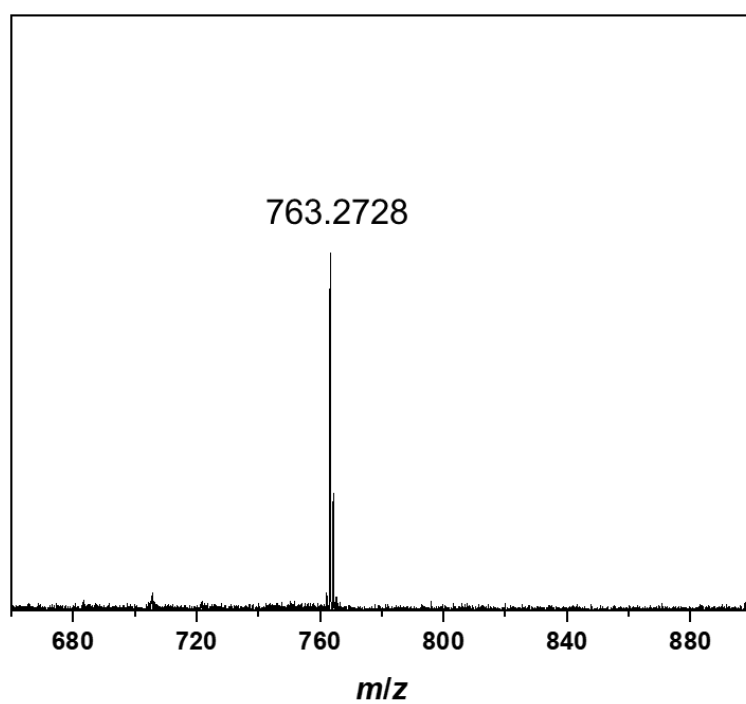


Figure S5. Maldi-TOF-MS of H_6L . Found $m/z = 763.2728$ $[H_6L+H]^+$, $C_{42}H_{30}N_6O_9$ requires $m/z = 763.2147$.

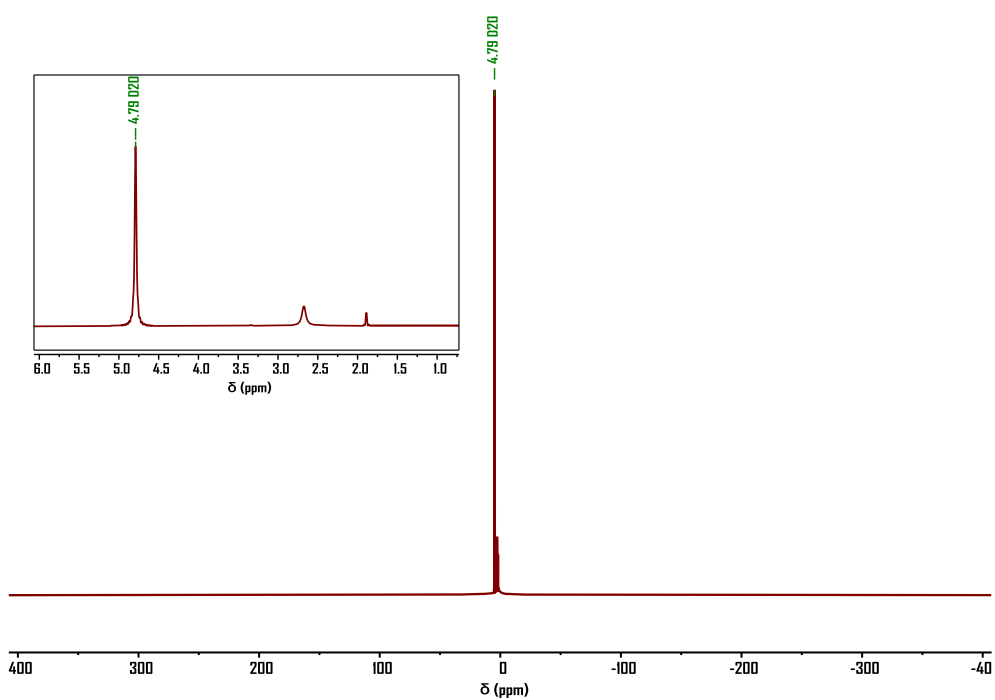


Figure S6. 1H NMR (400 MHz, $D_2O/DMSO-d_6 = 9/1$) of $(NEt_4)_{12}[Fe_4L_4]$.

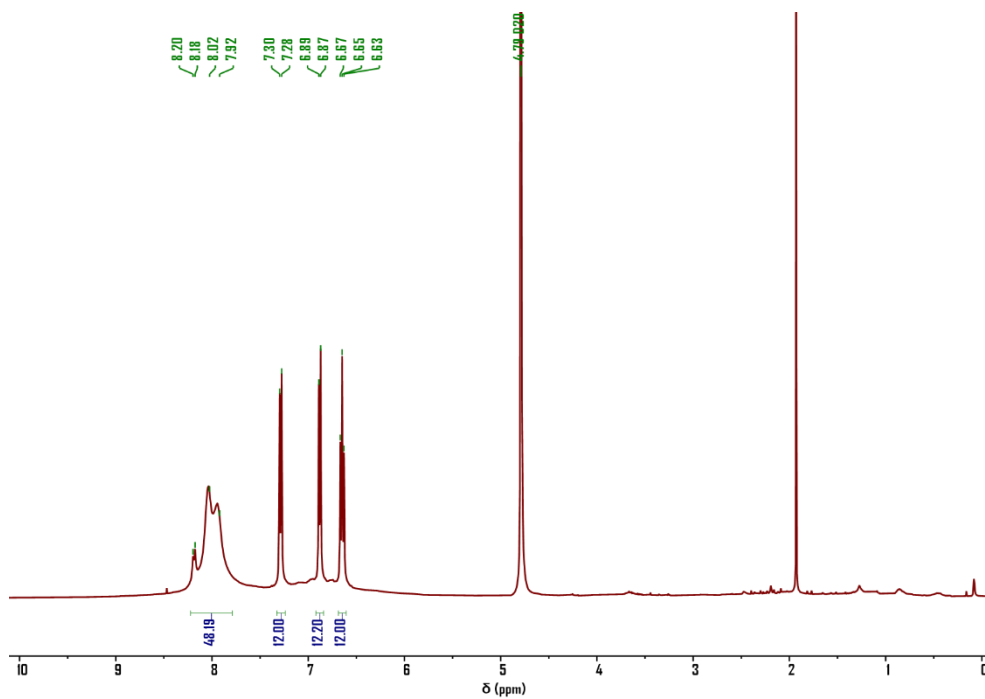


Figure S7. ^1H NMR (400 MHz, D_2O , 298K) spectrum of $\text{K}_{12}[\text{Ga}_4\text{L}_4]$.

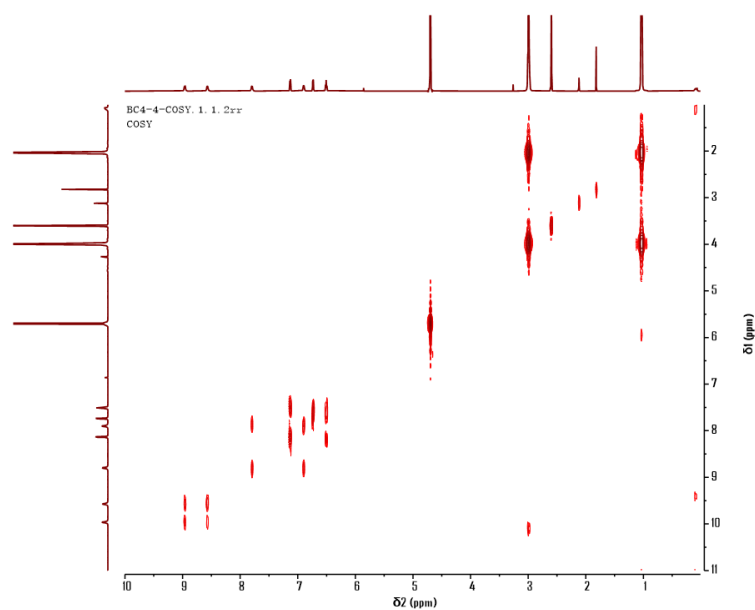


Figure S8. ^1H -COSY NMR (700 MHz, $\text{D}_2\text{O}/\text{DMSO-}d_6 = 9/1$) of $(\text{NEt}_4)_{12}[\text{Ga}_4\text{L}_4]$.

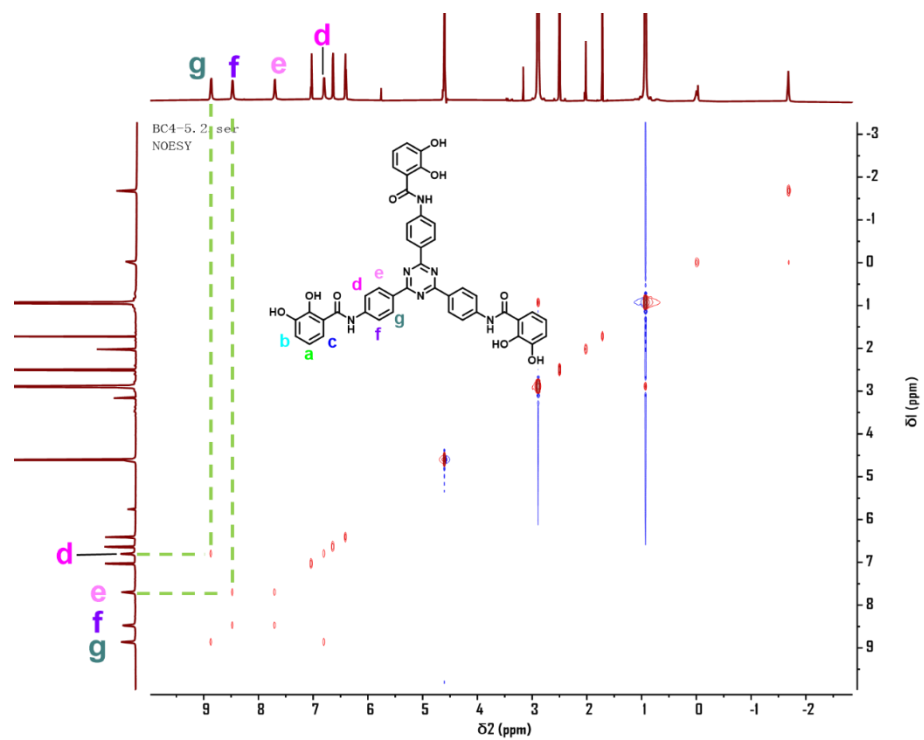


Figure S9. ^1H -NOESY NMR (700 MHz, $\text{D}_2\text{O}/\text{DMSO-}d_6 = 9/1$) of $(\text{NEt}_4)_{12}[\text{Ga}_4\text{L}_4]$.

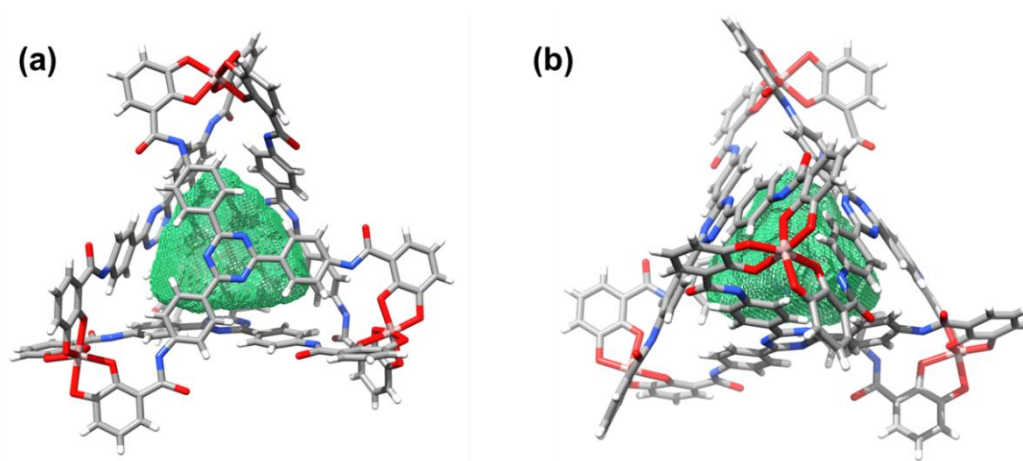


Figure S10. Crystal structure of $[\text{Ga}_4\text{L}_4]^{12-}$ showing the cavity as calculated using VOIDOO.

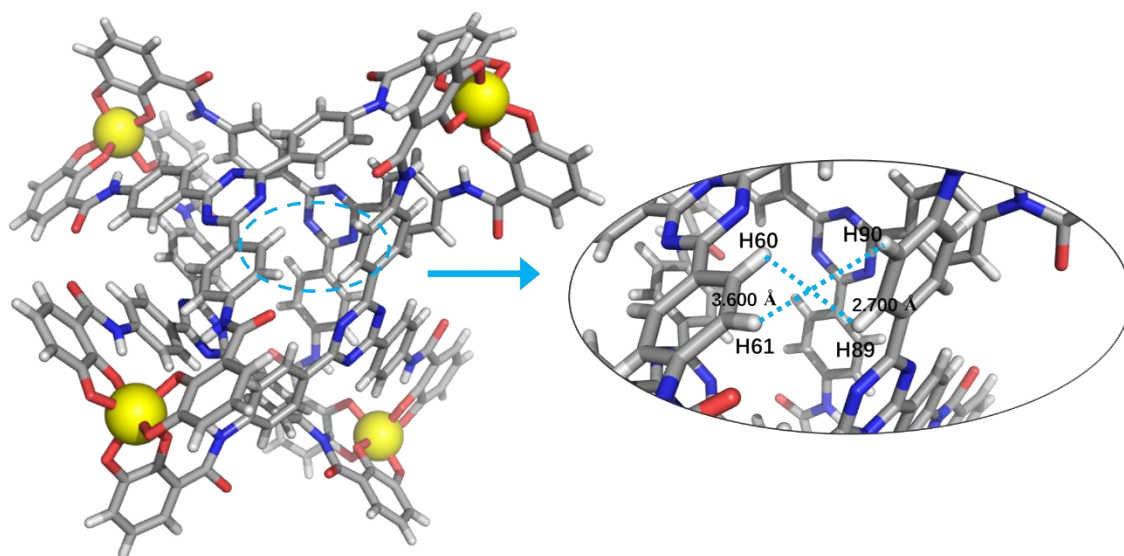


Figure S11. Illustration of the NOE interactions present in the crystal structure of $(\text{NEt})_{12}[\text{Ga}_4\text{L}_4]$.

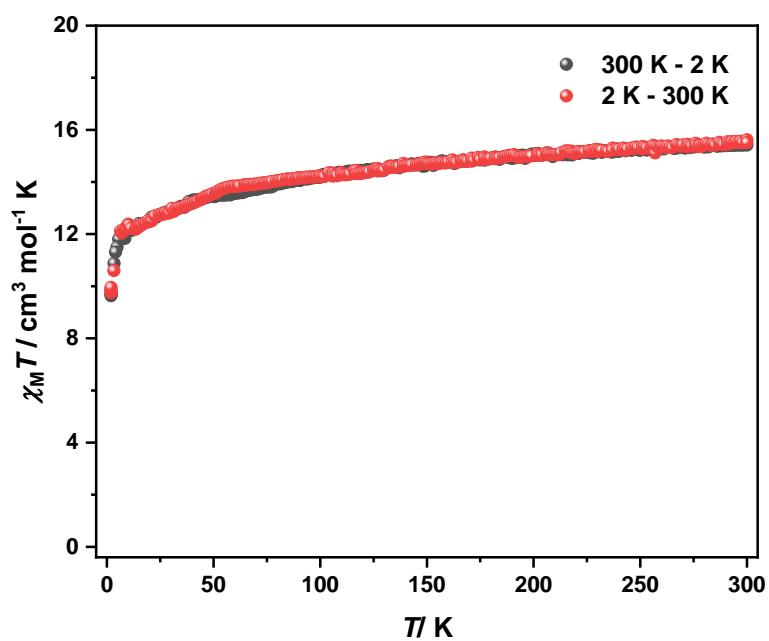


Figure S12. Variable-temperature magnetic susceptibility data for $\text{K}_{12}[\text{Fe}_4\text{L}_4]$ collected at 5000 Oe.

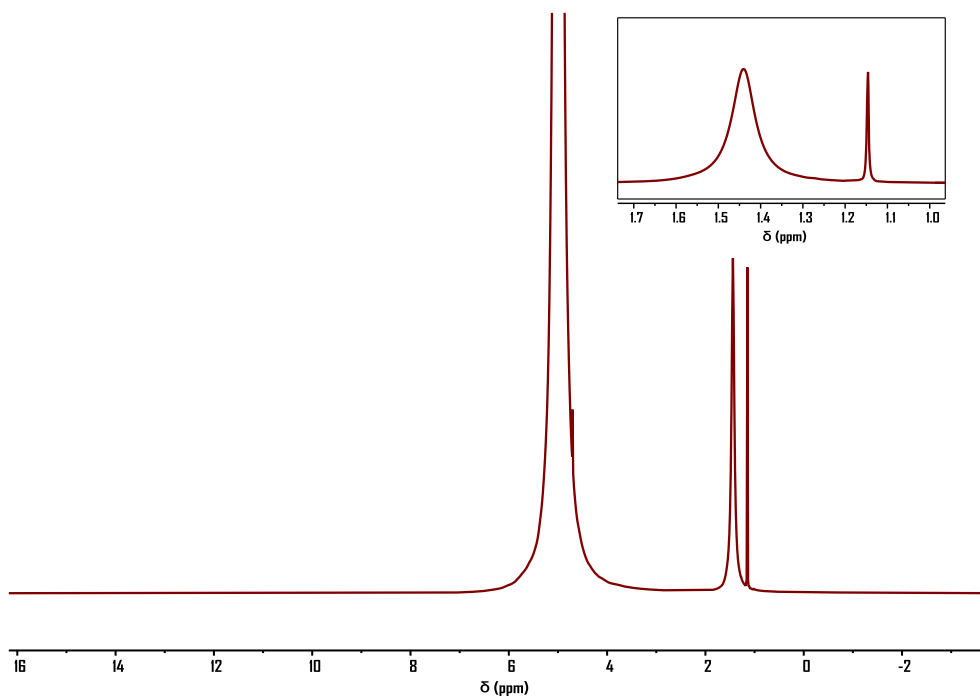


Figure S13. Magnetic measurement of 1.44 mM $K_{12}[Fe_4L_4]$ solution 5% t-butanol in PBS buffer at 298 K using Evans' method.

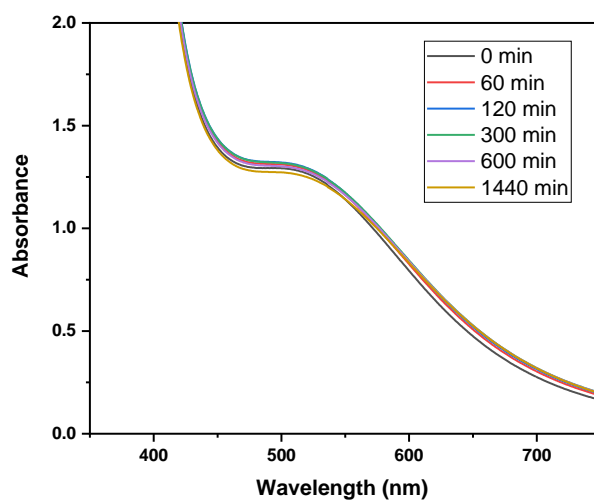


Figure S14. UV-Vis spectra of 100 μ M $K_{12}[Fe_4L_4]$ in HEPES Buffer with 100 mmol NaCl pH 7.4 at 37 $^{\circ}$ C over 1440 minutes with 40 equivalents of $Zn(NO_3)_2$.

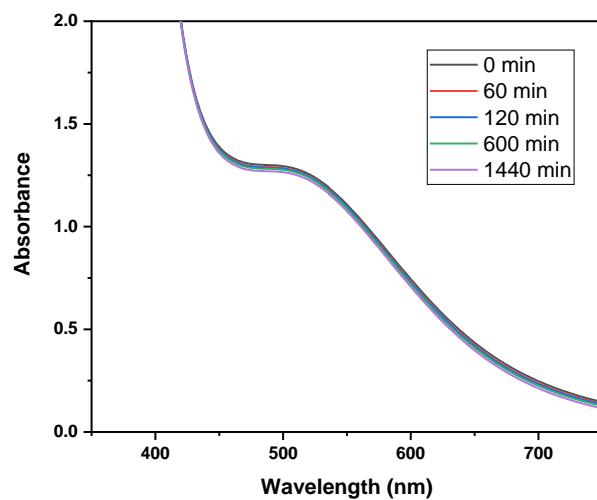


Figure S15. UV-Vis spectra of 100 μM K₁₂[Fe₄L₄] in HEPES Buffer with 100 mmol NaCl pH 7.4 at 37 °C over 1440 minutes with 4 equivalents of EDTA.

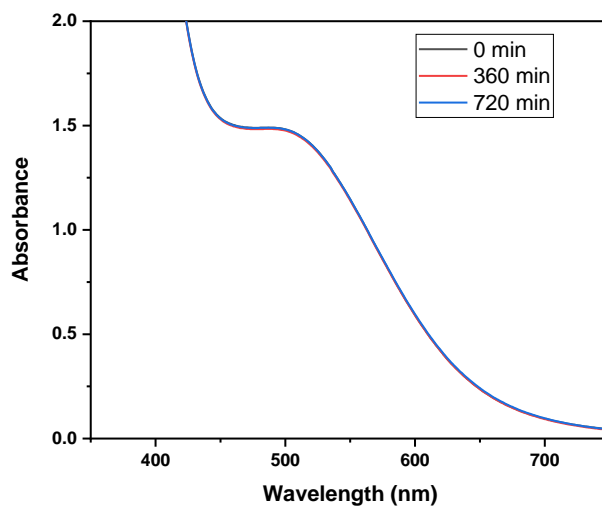


Figure S16. UV-Vis spectra of 100 μM K₁₂[Fe₄L₄] in 1 × PBS pH 7.4 at 37 °C over 720 minutes.

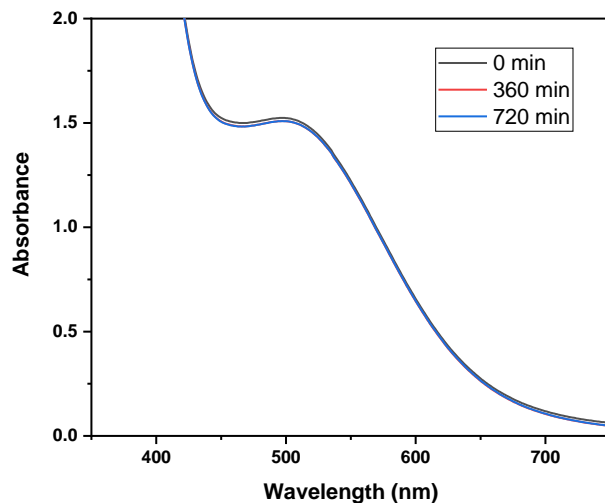


Figure S17. UV-Vis spectra of 100 μM K₁₂[Fe₄L₄] in PBS pH 7.4 at 37 °C with HSA (35mg/ mL) over 720 minutes.

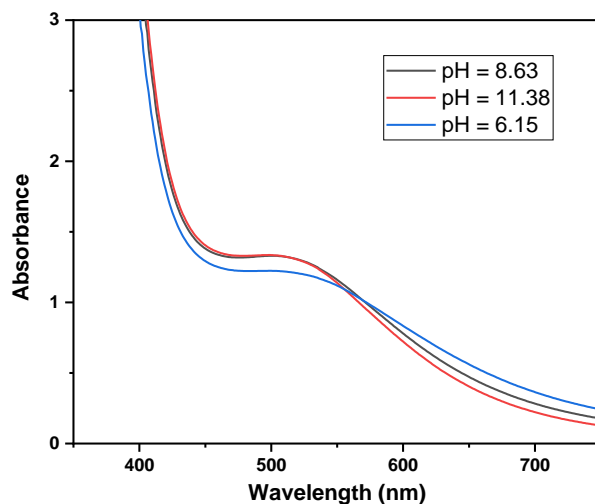


Figure S18. UV-Vis spectra of 100 μM K₁₂[Fe₄L₄] in water at different pHs of 8.63, 11.38 and 6.15, respectively.

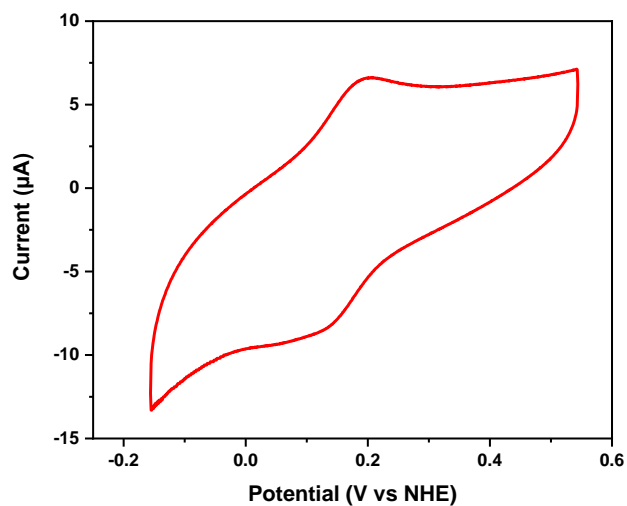


Figure S19. Cyclic voltammetric curve of 150 μM $\text{K}_{12}[\text{Fe}_4\text{L}_4]$ in 100 mM NaCl.

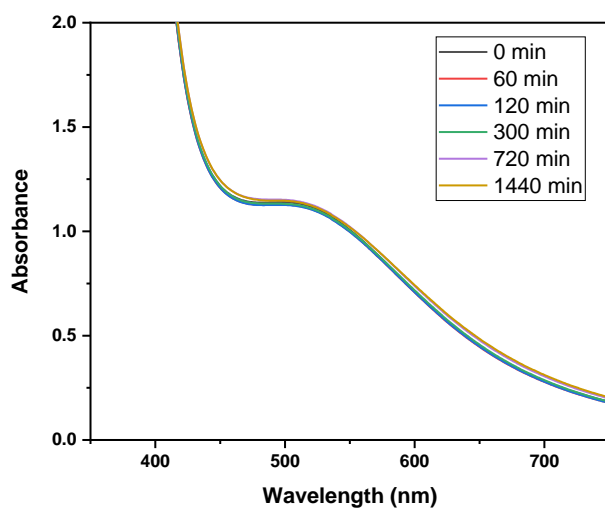


Figure S20. UV-Vis spectra of 100 μM $\text{K}_{12}[\text{Fe}_4\text{L}_4]$ in PBS pH 7.4 at 37 °C over 1440 minutes with 10 equivalents of ascorbic acid.

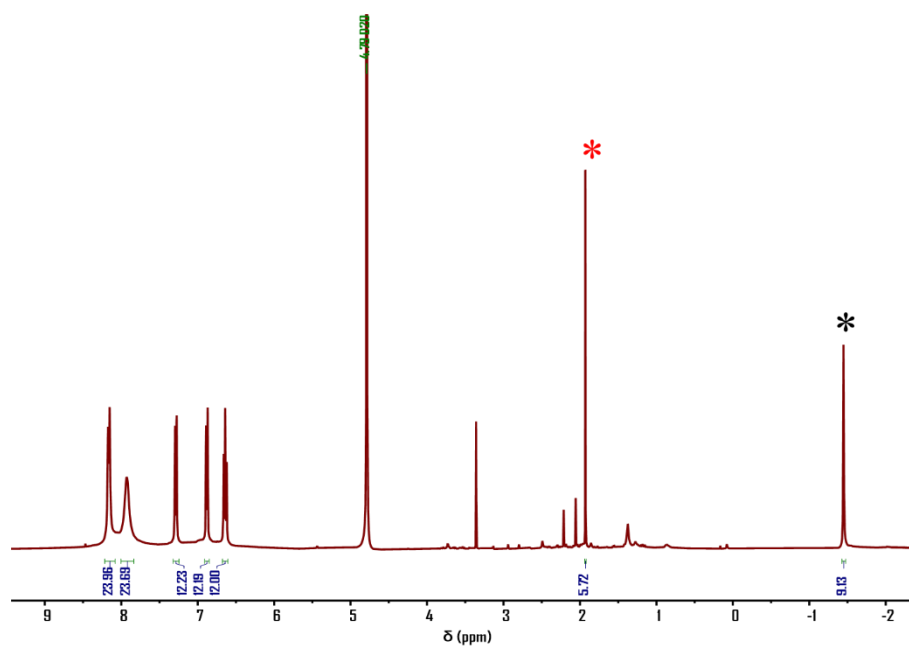


Figure S21. ¹H NMR spectrum of [cyclohexane-CGa₄L₄]¹²⁻ (D₂O, 400 MHz, 298 K) (*bound cyclohexane, *free cyclohexane).

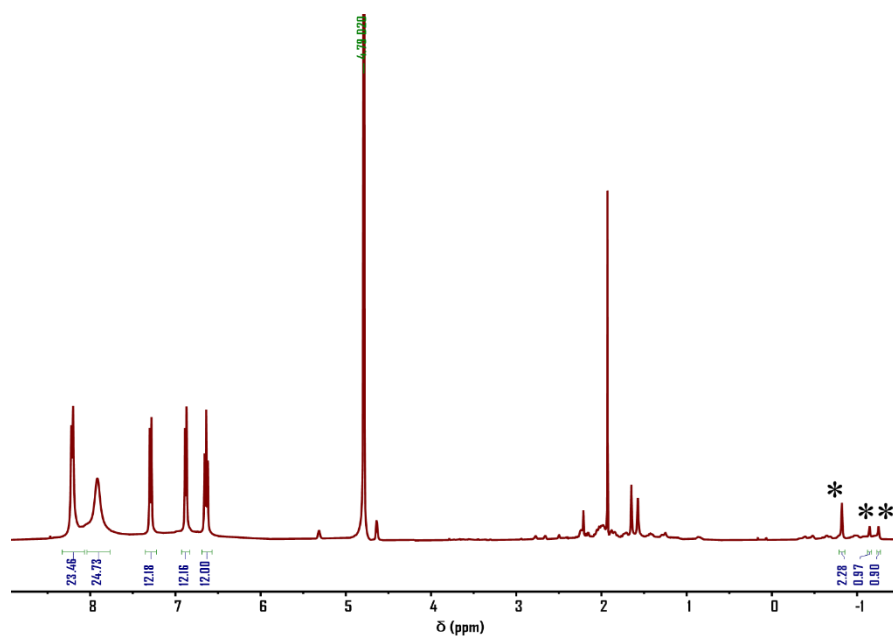


Figure S22. ¹H NMR spectrum of [(R)-limonene-CGa₄L₄]¹²⁻ (D₂O, 700 MHz, 298 K) (*bound (R)-limonene).

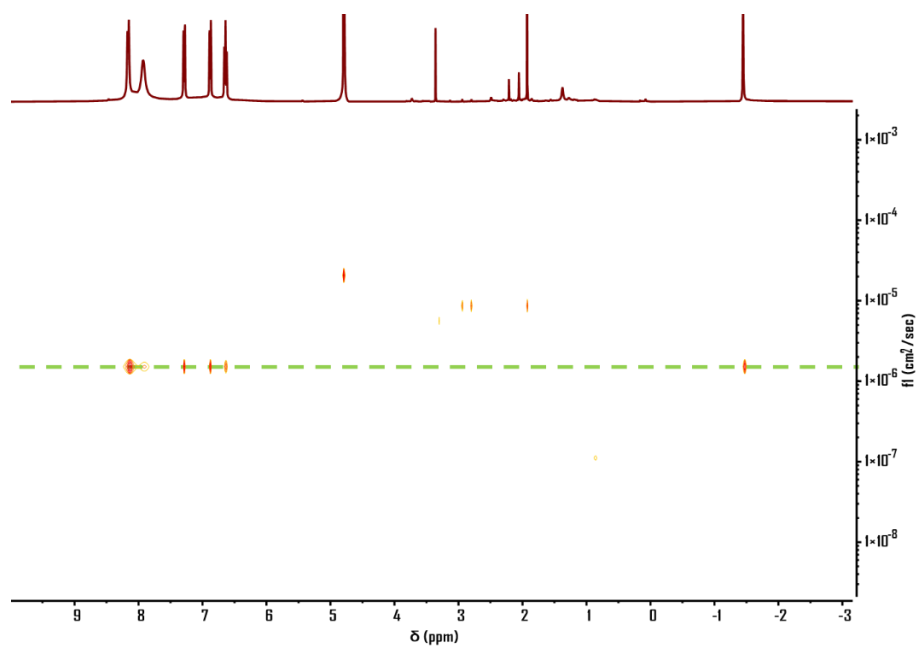


Figure S23. DOSY NMR spectrum of [cyclohexane⊂Ga₄L₄]¹²⁻ (D₂O, 700 MHz, 298 K).

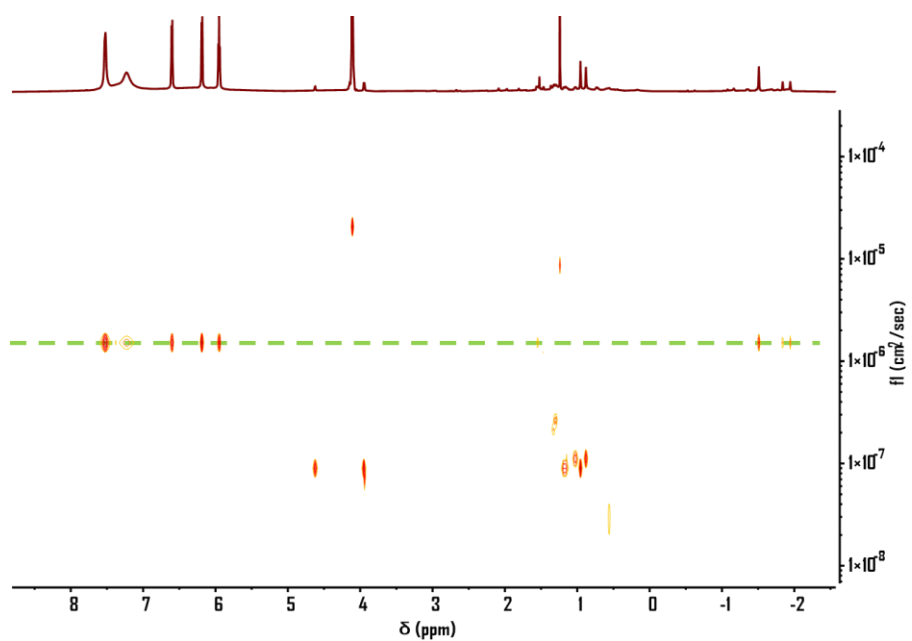


Figure S24. DOSY NMR spectrum of [(R)-limonene⊂Ga₄L₄]¹²⁻ (D₂O, 700 MHz, 298 K).

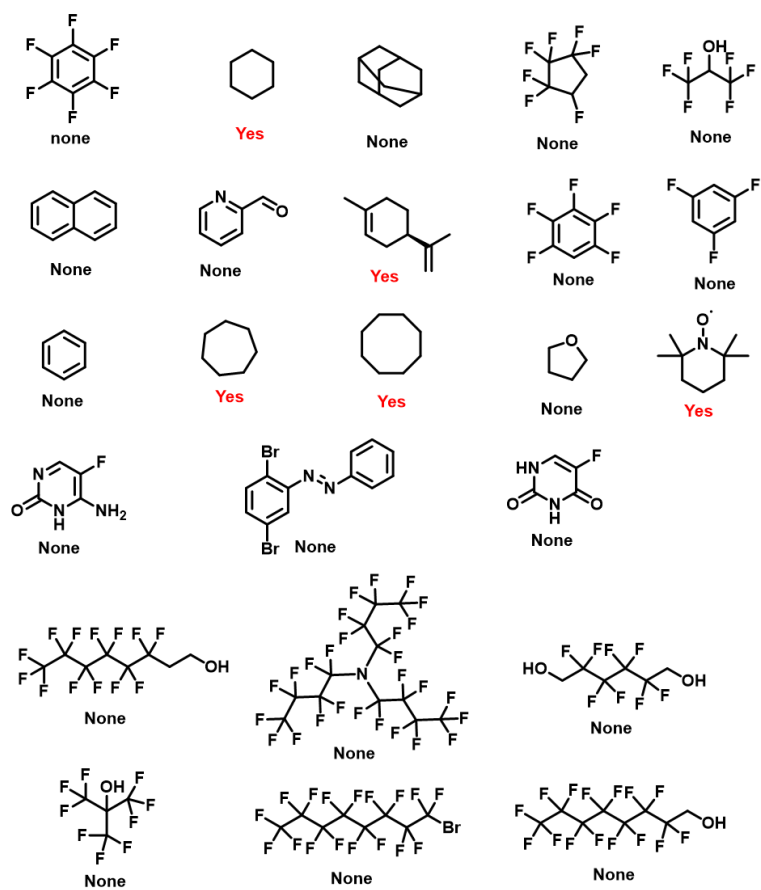


Figure S25. Attempted guest molecules for $K_{12}[Ga_4L_4]$ in D_2O .

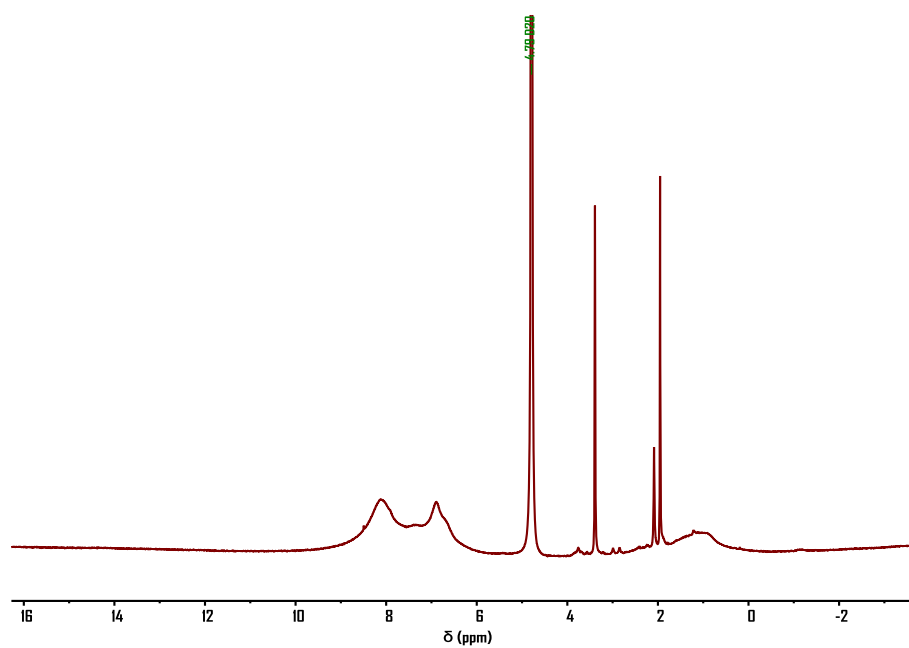


Figure S26. ^1H NMR spectrum of $[\text{TEMPO}\text{-Ga}_4\text{L}_4]^{12-}$ (D_2O , 400 MHz, 298 K).

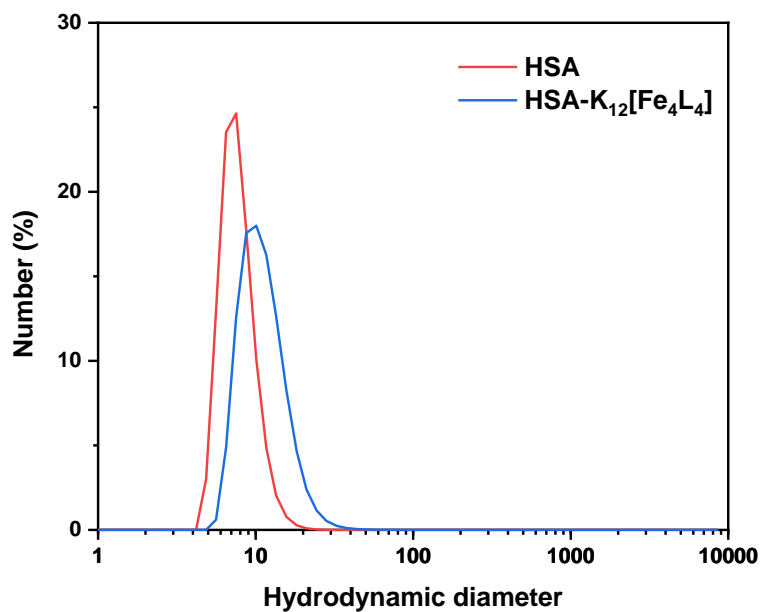


Figure S27. The hydrodynamic diameter of HSA and HSA upon mixing with $\text{K}_{12}[\text{Fe}_4\text{L}_4]$, respectively.

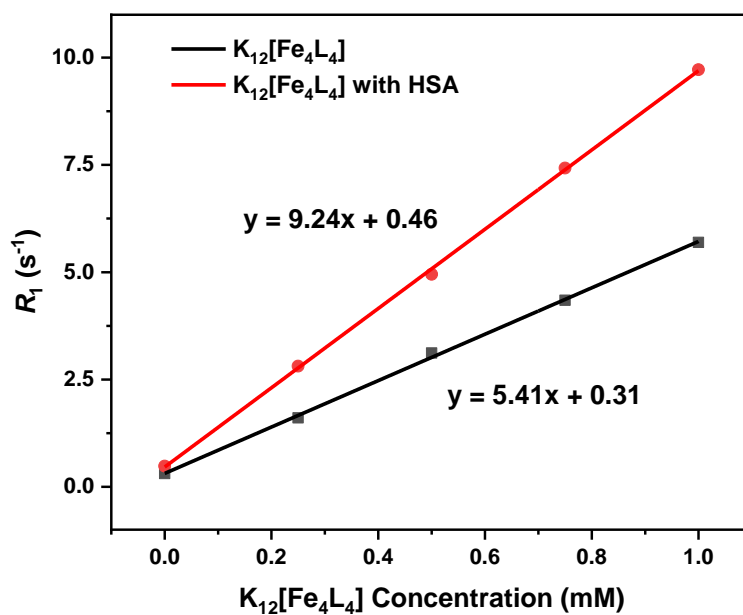


Figure S28. The longitudinal relaxivity r_1 of $\text{K}_{12}[\text{Fe}_4\text{L}_4]$ normalised to cage in pH = 7.4 PBS buffer at a field of 0.5 T and 32 °C both without and with HSA.

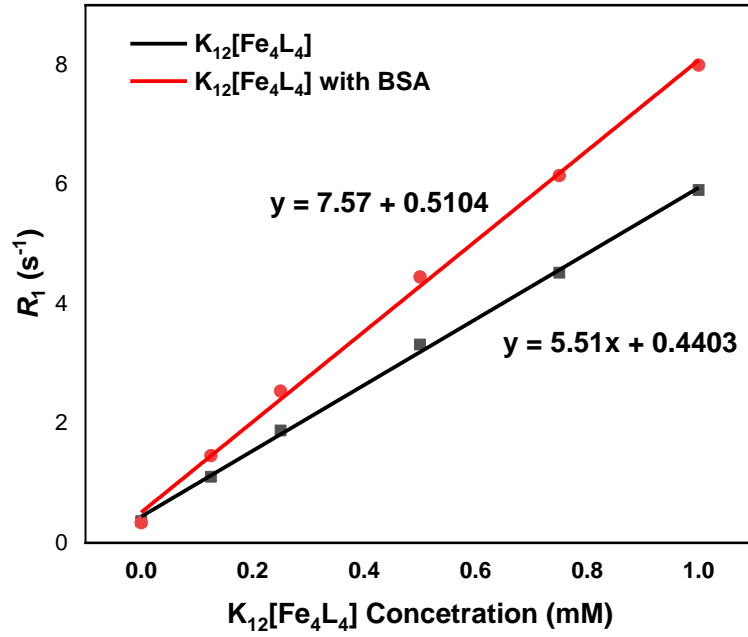


Figure S29. Proton longitudinal relaxivity r_1 of $K_{12}[Fe_4L_4]$ normalised to cage in PBS buffer pH of 7.4 at a field of 9.4 T and 22 °C both without and with HSA.

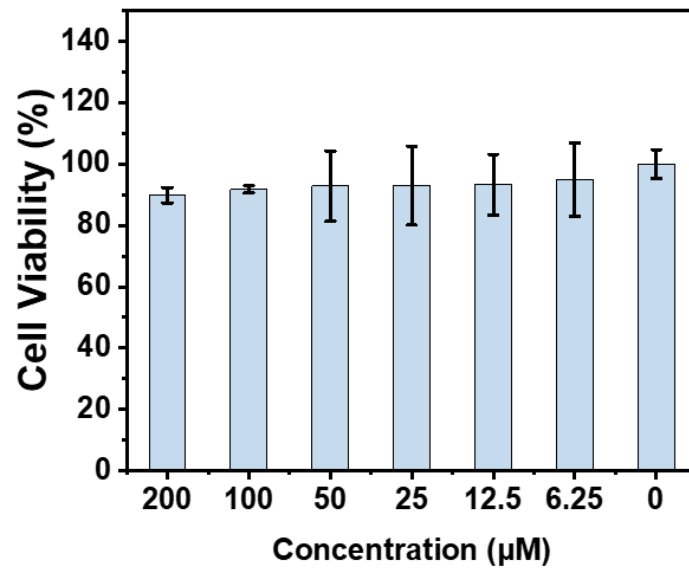


Figure S30. *In vitro* cytotoxicity: cell viability for Mlg2908 cells after incubation with $K_{12}[Fe_4L_4]$ for 12 h cell.

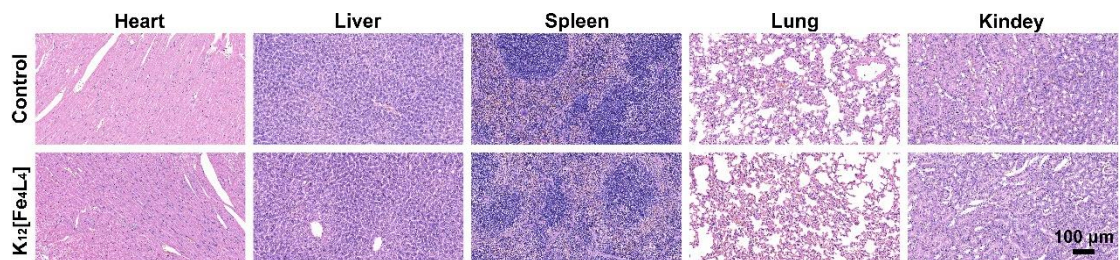


Figure S31. Histological images of H&E staining obtained from major organs (heart, liver, spleen, lung, and kidney) of mice after *i.v.* injection of $K_{12}[Fe_4L_4]$ (0.01 mM/kg) or physiological saline (control) for 24 h.

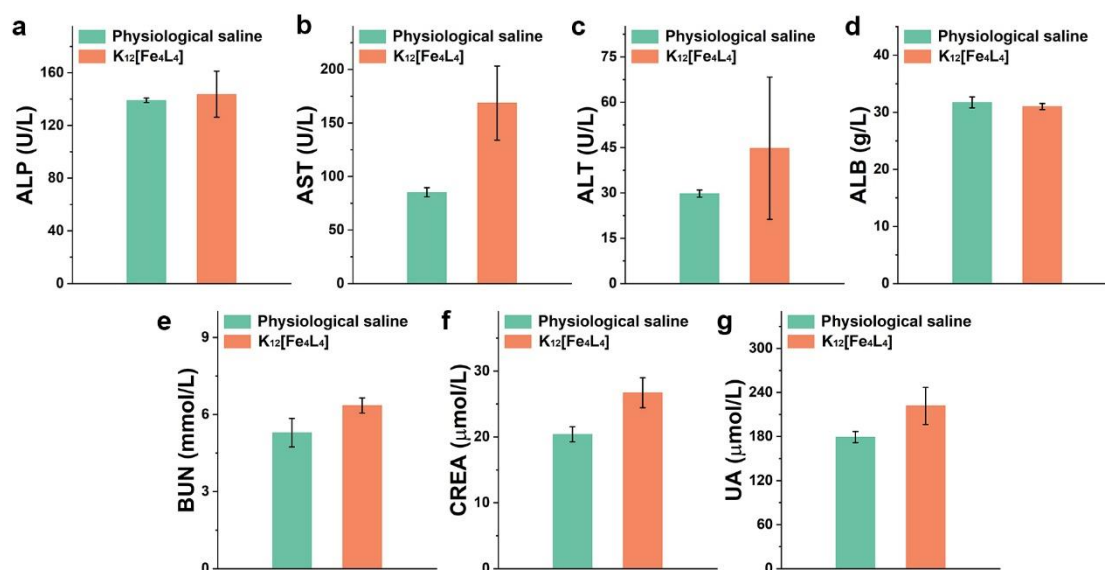


Figure S32. Blood indexes of ALP, AST, ALT, ALB, BUN, CREA, and UA of mice after *i.v.* injection of $K_{12}[Fe_4L_4]$ (0.01 mM/kg) or physiological saline for 24 h (mean \pm SD, $n = 3$).

4. References

- 1 S. Stoll and A. Schweiger, *J. Magn. Reson.*, 2006, **178**, 42-55.
- 2 G. M. Sheldrick, *Acta Crystallogr. C*, 2015, **71**, 3-8.
- 3 O. V. Dolomanov, L. J. Bourhis, R. J. Gildea, J. A. K. Howard and H. Puschmann, *J. Appl. Crystallogr.*, 2009, **42**, 339-341.
- 4 G. J. Kleywegt and T. A. Jones, *Acta Crystallogr. D*, 1994, **50**, 178-185.
- 5 Y. R. Hristova, M. M. J. Smulders, J. K. Clegg, B. Breiner and J. R. Nitschke, *Chem. Sci.*, 2011, **2**, 638-641.